frontiers | Frontiers in Physics

TYPE Original Research
PUBLISHED 26 January 2023
DOI 10.3389/fphy.2023.1111163



OPEN ACCESS

EDITED BY
Bhaskar Chaudhury,
Dhirubhai Ambani Institute of Information and Communication Technology, India

REVIEWED BY
Nehad Ali Shah,
Sejong University, South Korea
M. M. Bhatti,
Shandong University of Science and Technology, China

*CORRESPONDENCE
Nouman Ijaz,
noumanijaz666@gmail.com
Arshad Riaz,
arshad-riaz@ue.edu.pk

SPECIALTY SECTION
This article was submitted to Statistical and Computational Physics, a section of the journal Frontiers in Physics

RECEIVED 29 November 2022
ACCEPTED 04 January 2023
PUBLISHED 26 January 2023

CITATION
Fatima N, Abdulkhaliq M. Alharbi K, Ijaz N, Riaz A and El-Din EMT (2023), Analysis of rotating-symmetric frame and MHD for peristaltic multiphase flow: An exact solution.
*Front. Phys.* 11:1111163.
doi: 10.3389/fphy.2023.1111163



# RETRACTED: Analysis of rotating-symmetric frame and MHD for peristaltic multiphase flow: An exact solution

Nahid Fatima[1], Khalid Abdulkhaliq M. Alharbi[2], Nouman Ijaz[3]*, Arshad Riaz[4]* and ElSayed M. Tag El-Din[5]

[1]Department of Mathematics and Sciences, Prince Sultan University, Riyadh, Saudi Arabia, [2]Mechanical Engineering Department, College of Engineering, Umm Al-Qura University, Makkah, Saudi Arabia, [3]Department of Mathematics and Statistics, Punjab Group of Colleges, Jhelum, Pakistan, [4]Department of Mathematics, Division of Science and Technology, University of Education, Lahore, Pakistan, [5]Center of Research, Faculty of Engineering, Future University in Egypt, New Cairo, Egypt



The rotational mechanism forms the basis of various cosmic and geophysical transports. In medical science, rotational blood flows have been related to healthy cardiac function. This study consists of a mathematical model representing magnetohydrodynamic effects on the two-phase pumping flow of a Ree–Eyring–Powell stress model in a rotating frame. The model is controlled by switching the system into a wave frame of reference for better analysis of the wave phenomenon. Moreover, a lubrication theory is applied to the resulting set of relations in order to get a more comprehensive form of the reduced mathematical model. In the end, an exact solution is found to discuss the substantial contents of the study. The data on velocity and stream function are presented diagrammatically to examine the theoretical behavior of various quantities under the variation of considerable physical factors. It is concluded from the graphs that axial and secondary velocities are decreasing against rotation, magnetic field, and fluid's factor, but the same rise in the case of wall stiffness and particle concentration. In both industrial and biomedical applications, this type of flow measurement gives tomographic information on the multiphase flow process, which entails acquiring signal changes at the edges of objects like fluid pipes or blood vessels to determine how the objects are distributed within. This work is extendable by considering nanoparticles of various types to enhance the thermal conductivity of the flow.

KEYWORDS

**multiphase flow, Ree–Eyring–Powell model, peristaltic movement, rotating frame, magnetohydrodynamics, exact solutions, compliant walls**

## 1 Introduction

Peristalsis is a type of flow where a fluid is moved as a series of waves produced through the evolution and contraction of a conduit's walls. Many human organs exhibit this behavior, including the esophagus where food is moved, the arteries where blood is pumped by the heart, and the bladder where urine is transported from the kidney. Leeches possess the ability to suck blood and propel it through the body by pumping in wavy patterns and are frequently used in the curing of tumors, cerebral disease, and skin problems by extracting affected blood cells from the infected portion of the body. Transfer of sanitary liquids, toxic fluid streams in nuclear assembling, and movement of corrosive substances are only a few industrial instances where peristaltic flow processes are useful. The majority of medical devices, including heart–lung machines and blood

pumps, employ this strategy. The fundamental concepts and the significance of the many physical features of the flow phenomena were discussed by Shapiro et al. [1]. On the basis of the presumptions of broad wavelengths and low Reynolds numbers, surveys of interpretative research and theories on the peristaltic movements of various flow structures have been thoroughly discussed and described in open letters. Due to its widespread employment in numerous industrial sectors and also clinical problems, this topic is the focus of a large number of scientific researchers and biologists. Numerous geometries, including two- and three-dimensional channels, pipes, annulus, curved conduits, and ducts, have been used in the research. The recent studies on the subject are the primary focus of this paper. Rao and Mishra [2] considered the pumping effects on the flow of Newtonian fluids assumed in an asymmetric channel and incorporated curvature properties. They produced a result based on their findings that asymmetry executes a vital contribution in performing mixing. Munawar et al. [3] discussed the viscous fluid pumping characteristics in a symmetric enclosure by taking various viscosity models and declared that such models of viscosity can be useful in reducing the system entropy. Pandey and Tripathi [4] presented analytical results for the viscous fluid taken in a cylindrical conduit along with the properties of the magnetic field. The authors have suggested through their graphical aspects that the integral number of peristaltic waves keeps the pressure unchanged, while the non-integral number of such waves produces different pressure curve heights. Sadaf and Nadeem [5] analyzed convective dissipation and viscous effects for the pumping stream of a non-linear fluid model by considering wall properties. The study revealed that the parameter controlling viscous dissipation works by increasing the system temperature and compliant nature of the walls enlarges the flow speed for shear-thinning rheological properties of the fluid. Some similar studies can be reported in [6–10].

The magnetohydrodynamic (MHD) transport of a liquid in an elastic channel with systematically contracting boundaries is of great attraction in relation to some issues with the movement of conductive physiological fluids, for example, the blood, and with the requirement for theoretical research on the operation of the peristaltic MHD compressor. Additionally, the magnetic field's influence could be used as a blood pump during cardiac procedures to improve blood flow in arteries affected by arterial diseases such as arterial stenosis or arteriosclerosis. Khan et al. [11] discussed the peristaltic flow of nanofluids with magnetic field induction through an asymmetric enclosure. In this study, three various shapes of nanoparticles are assumed. Authors have gained numerical data from the study and found that cylindrical particles have low thermal conductivity as compared to other shapes. Sucharitha et al. [12] considered heating and wall effects for the peristaltic stream of the nanofluid along with MHD and proved that the fluid travels with high speed in a diverging channel as contrasted with the uniform one, but this is not the case for temperature and concentration profiles. Srinivas and Kothandapani [13] produced the results for heat and mass analysis in a peristaltic transport along a porous conduit including the magnetic field and walls' compliance. This study is conducted under the constraints of the low Reynolds number and small wave number. The results are found numerically and explained graphically. The results declare that the Schmidt number expresses an inverse relationship with the concentration. Some more works on the field can be cited in [14–18].

The rotational phenomenon forms the basis of many cosmic and geophysical flows. Studying and comprehending the behavior of ocean circulation and galaxy formation is made easier by rotation. Hayat et al. [19] presented entropy generation effects in the wavy flow of nanofluids in the rotating frame of reference by imposing an external magnetic field. The study reveals that temperature is reduced for the high rate of radiation effects, but the entropy rate is increased. Hasen and Abdulhadi [20] published rotating inclined channel effects on pumping characteristics of a non-Newtonian fluid through heat exchange effects and declared that axial and secondary velocities and temperature are directly dependent on the rotational factor. Haider et al. [21] executed the rotational and MHD effects on the dual-phase flow in a rotating enclosure with peristaltic movements. It is observed from the readings that the fluid's velocity decreases with the rotation factor and magnetic field, but the particle volume fraction exerts a direct impact on the said profile. Mabood et al. [22] considered the nanofluid for peristaltic pumping of the Newtonian model in a rotating channel. In this study, data are evaluated numerically through the Keller box difference scheme and analyzed that thermophoresis parameters exerted a dominant impact in the rotating frame, as equated to the non-rotating frame. More studies on the rotating channel flow can be found in [23–28]. Rotational transport is linked with healthy heart performance [29]. Affected heart patients having swirling structures inside the left atrium suffer lesser organic cardiac diseases and high flow speeds contrasted to those whose flow entry collided, but this is not the case in rotational transport. The potential for blood stagnation is one issue with colliding flows, a major characteristic of the numerous cardiac diseases that are linked to thrombus formation [30–41]. As a result, it can be assumed that the rotational flow and the interplay of the SVC and IVC in the RA may also play a role. Once more, it is proposed that the vortex created in the LA might be related to increased effectiveness as blood is transferred from the pulmonary veins to the left ventricle (LV).

From the aforementioned literature survey, it is conveyed that researchers working on the topic of peristaltic pumping are highly committed to the study on the rotating frame, and also, the multiphase flows are a point of keen interest due to their immense applications in many industrial and medical field sectors. It is quite notable that none of the scientists and researchers has discussed the study of the multiphase flow in a rotating conduit by considering magnetic field effects for a Ree–Eyring–Powell fluid model. In the current work, authors are interested to work on the MHD flow of a Ree–Eyring–Powell fluid model in the rotating frame under the additional effects of solid particles. This sort of flow measurement provides tomographic information on the multiphase flow process in both industrial and biomedical applications. It does this by collecting signal changes at the borders of objects like fluid pipes or blood arteries to ascertain how the items are dispersed inside. The equations are maintained under the limitations to the long wavelength and the low Reynolds number. A wave frame is also introduced for transforming into another system with a simplified structure. An exact solution is derived by solving the system of differential equations. The results are drawn graphically to enable a reader to examine the variation effects of some pertinent factors on measurable quantities.

## 2 Model descriptions

The rotating channel phenomena of an incompressible and evenly distributed particle suspension in a Ree–Eyring stable and irrotational fluid moving at a velocity c are taken into consideration in this work. It is presumed that the substance is a reliable conductor of electricity. Perpendicular to the X-axis, a consent field caused by permanent magnetism is applied externally. As seen in Figure 1, the flow problem

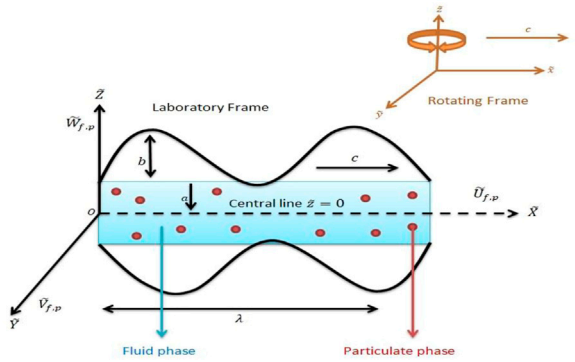


FIGURE 1
Geometry of the problem.

is illustrated in the Cartesian coordinate system with the X-axis, reflecting parallel with the flow, and the others admitted normal to it.

Mathematically, the wall function of Figure 1 is demonstrated as follows [21]:

$$h(x,t) = a + b\,Sin\left[\frac{2\pi}{\lambda}\left(\tilde{X} - ct\right)\right]. \tag{1}$$

We define the velocity vector as

$$\vec{V} = \langle \tilde{U}_{f,p}\left(\tilde{X},\tilde{Z},\tilde{t}\right), \tilde{V}_{f,p}\left(\tilde{X},\tilde{Z},\tilde{t}\right), \tilde{W}_{f,p}\left(\tilde{X},\tilde{Z},\tilde{t}\right)\rangle, \tag{2}$$

where the subscripts $f$ and $p$ stand for the fluid and particulate, respectively. The stress tensor of the Ree–Eyring fluid model is defined as [16, 21, 25]

$$\mathfrak{R}_{ij} = \mu_s \frac{\partial \tilde{V}_i}{\partial \tilde{x}_j} + \frac{1}{B} Sin\, h^{-1}\left(\frac{1}{C}\frac{\partial \tilde{V}_i}{\partial \tilde{x}_j}\right). \tag{3}$$

Since

$$Sinh^{-1} x \approx x \text{ of } |x| \le 1,$$

$$\mathfrak{R}_{ij} = \mu_s \frac{\partial \tilde{V}_i}{\partial \tilde{x}_j} + \frac{1}{B}\left(\frac{1}{C}\frac{\partial \tilde{V}_i}{\partial \tilde{x}_j}\right), \tag{4}$$

$$\frac{\partial \tilde{U}_f}{\partial \tilde{X}} + \frac{\partial \tilde{V}_f}{\partial \tilde{Y}} + \frac{\partial \tilde{W}_f}{\partial \tilde{Z}} = 0, \tag{5}$$

$$\left(\frac{\partial \tilde{U}_f}{\partial \tilde{t}} + \tilde{U}_f\frac{\partial \tilde{U}_f}{\partial \tilde{X}} + \tilde{W}_f\frac{\partial \tilde{U}_f}{\partial \tilde{Z}}\right) - \frac{2k\tilde{V}_f}{(1-C)}$$
$$= -\frac{\partial \tilde{P}}{\partial \tilde{X}} + \frac{\partial \mathfrak{R}_{\tilde{X}\tilde{X}}}{\partial \tilde{X}} + \frac{\partial \mathfrak{R}_{\tilde{X}\tilde{Y}}}{\partial \tilde{Y}} + \frac{\partial \mathfrak{R}_{\tilde{X}\tilde{Z}}}{\partial \tilde{Z}} + \frac{1}{1-C}\left(\tilde{U}_p - \tilde{U}_f\right) - \frac{\sigma B_0^2 \tilde{U}_f}{(1-C)}, \tag{6}$$

$$\left(\frac{\partial \tilde{V}_f}{\partial \tilde{t}} + \tilde{U}_f\frac{\partial \tilde{V}_f}{\partial \tilde{X}} + \tilde{W}_f\frac{\partial \tilde{V}_f}{\partial \tilde{Z}}\right) + \frac{2k\tilde{V}_f}{(1-C)}$$
$$= -\frac{\partial \tilde{P}}{\partial \tilde{Y}} + \frac{\partial \mathfrak{R}_{\tilde{Y}\tilde{X}}}{\partial \tilde{X}} + \frac{\partial \mathfrak{R}_{\tilde{Y}\tilde{Y}}}{\partial \tilde{Y}} + \frac{\partial \mathfrak{R}_{\tilde{Y}\tilde{Z}}}{\partial \tilde{Z}} + \frac{1}{1-C}\left(\tilde{V}_p - \tilde{V}_f\right), \tag{7}$$

$$\left(\frac{\partial \tilde{W}_f}{\partial \tilde{t}} + \tilde{U}_f\frac{\partial \tilde{W}_f}{\partial \tilde{X}} + \tilde{W}_f\frac{\partial \tilde{W}_f}{\partial \tilde{Z}}\right) = -\frac{\partial \tilde{P}}{\partial \tilde{Z}} + \frac{\partial \mathfrak{R}_{\tilde{Z}\tilde{X}}}{\partial \tilde{X}} + \frac{\partial \mathfrak{R}_{\tilde{Z}\tilde{Y}}}{\partial \tilde{Y}} + \frac{\partial \mathfrak{R}_{\tilde{Z}\tilde{Z}}}{\partial \tilde{Z}}$$
$$+ \frac{1}{1-C}\left(\tilde{W}_p - \tilde{W}_f\right), \tag{8}$$

$$\frac{\partial \tilde{U}_p}{\partial \tilde{X}} + \frac{\partial \tilde{V}_p}{\partial \tilde{Y}} + \frac{\partial \tilde{W}_p}{\partial \tilde{Z}} = 0, \tag{9}$$

$$\left(\frac{\partial \tilde{U}_p}{\partial \tilde{t}} + \tilde{U}_p\frac{\partial \tilde{U}_p}{\partial \tilde{X}} + \tilde{W}_p\frac{\partial \tilde{U}_p}{\partial \tilde{Z}}\right) = -\frac{\partial \tilde{P}}{\partial \tilde{X}} + \frac{1}{1-C}\left(\tilde{U}_p - \tilde{U}_f\right), \tag{10}$$

$$\left(\frac{\partial \tilde{V}_f}{\partial \tilde{t}} + \tilde{U}_f\frac{\partial \tilde{V}_f}{\partial \tilde{X}} + \tilde{W}_f\frac{\partial \tilde{V}_f}{\partial \tilde{Z}}\right) = -\frac{\partial \tilde{P}}{\partial \tilde{Y}} + \frac{1}{1-C}\left(\tilde{V}_p - \tilde{V}_f\right), \tag{11}$$

$$\left(\frac{\partial \tilde{W}_f}{\partial \tilde{t}} + \tilde{U}_f\frac{\partial \tilde{W}_f}{\partial \tilde{X}} + \tilde{W}_f\frac{\partial \tilde{W}_f}{\partial \tilde{Z}}\right) = -\frac{\partial \tilde{P}}{\partial \tilde{Z}} + \frac{1}{1-C}\left(\tilde{W}_p - \tilde{W}_f\right) \tag{12}$$

.

Let us describe the linear transformations based on the shift from the fixed system to the moving wave frame:

$$\begin{aligned} \tilde{x} &= \tilde{X} - c\tilde{t},\ \tilde{y} = \tilde{Y},\ \tilde{z} = \tilde{Z}, \\ \tilde{u}_{f,p} &= \tilde{U}_{f,p} - c,\ \tilde{v}_{f,p} = \tilde{V}_{f,p}, \\ \tilde{w}_{f,p} &= \tilde{W}_{f,p},\ \tilde{p}(x,y,z) = \tilde{P}(X,Y,Z). \end{aligned} \tag{13}$$

Defining the non-dimensional quantities

$$x = \tilde{x}\lambda^{-1}, y = \tilde{y}d^{-1}, z = \tilde{z}a^{-1}, u_{f,p} = \tilde{u}_{f,p}c^{-1}, w_{f,p} = \tilde{w}_{f,p}(c\delta)^{-1},$$
$$t = c\tilde{t}\lambda^{-1}, \tilde{h}, = Ha^{-1}, \varphi = ba^{-1}, p = a^2\tilde{p}(uc\lambda)^{-1}, \delta = a\lambda^{-1},$$
$$\beta = ad^{-1}, \mathrm{Re} = \rho ac\delta\mu^{-1}, M_1 = S'a^2\mu_s^{-1}(1-C)^{-1},$$
$$M = \sqrt{\sigma\mu^{-1}}a\beta_0, \alpha' = (\mu_s BC)^{-1}, \bar{k} = ka^{-2}, \mathfrak{R}_{xx} = \tilde{\mathfrak{R}}_{\tilde{x}\tilde{x}}a(uc)^{-1},$$
$$\mathfrak{R}_{xz} = \tilde{\mathfrak{R}}_{\tilde{x}\tilde{z}}a(uc)^{-1}, \mathfrak{R}_{xy} = \tilde{\mathfrak{R}}_{\tilde{x}\tilde{y}}d(uc)^{-1}, \mathfrak{R}_{yz} = \tilde{\mathfrak{R}}_{\tilde{y}\tilde{z}}d(uc)^{-1},$$
$$\mathfrak{R}_{yy} = \tilde{\mathfrak{R}}_{\tilde{y}\tilde{y}}\lambda(uc)^{-1}, \mathfrak{R}_{zz} = \tilde{\mathfrak{R}}_{\tilde{z}\tilde{z}}\lambda(uc)^{-1}. \tag{14}$$

Now, Eqs 5–12 after making use of Eqs 13, 14 become

$$\frac{\partial u_f}{\partial x} + \frac{\partial w_f}{\partial z} = 0, \tag{15}$$

$$\mathrm{Re}\left(u_f\frac{\partial u_f}{\partial x} + w_f\frac{\partial u_f}{\partial z}\right) - \frac{2\kappa' v_f}{(1-C)} = -\frac{\partial p}{\partial x} + \delta^2\frac{\partial \mathfrak{R}_{xx}}{\partial x} + \frac{\partial \mathfrak{R}_{xy}}{\partial y} + \frac{\partial \mathfrak{R}_{xz}}{\partial z}$$
$$+ M_1 C\left(u_p - u_f\right) - \frac{M^2\left(u_f + 1\right)}{(1-C)}, \tag{16}$$

$$\mathrm{Re}\left(u_f\frac{\partial v_f}{\partial x} + w_f\frac{\partial v_f}{\partial z}\right) + \frac{2\kappa' v_f}{(1-C)} = -\frac{\partial p}{\partial y} + \delta^2\frac{\partial \mathfrak{R}_{yx}}{\partial x} + \frac{\partial \mathfrak{R}_{yy}}{\partial y} + \frac{\partial \mathfrak{R}_{yz}}{\partial z}$$
$$+ M_1 C\left(v_p - v_f\right), \tag{17}$$

$$\mathrm{Re}\delta^2\left(u_f\frac{\partial w_f}{\partial x} + w_f\frac{\partial w_f}{\partial z}\right) = -\frac{\partial p}{\partial z}$$
$$+\delta^2\left(\delta^2\frac{\partial \mathfrak{R}_{zx}}{\partial x} + \frac{\partial \mathfrak{R}_{zy}}{\partial y} + \frac{\partial \mathfrak{R}_{zz}}{\partial z} + M_1 C\left(w_p - w_f\right)\right), \tag{18}$$

$$\frac{\partial u_p}{\partial x} + \frac{\partial w_p}{\partial z} = 0, \tag{19}$$

$$\mathrm{Re}\left(u_p\frac{\partial u_p}{\partial x} + w_p\frac{\partial u_p}{\partial z}\right) = \frac{\partial p}{\partial x} + M_1(1-C)\left(u_f - u_p\right), \tag{20}$$

$$\mathrm{Re}\delta\left(u_p\frac{\partial v_p}{\partial x} + w_p\frac{\partial v_p}{\partial z}\right) = \frac{\partial p}{\partial y} + M_1\delta(1-C)\left(v_f - v_p\right), \tag{21}$$

$$\mathrm{Re}\delta\left(u_p\frac{\partial w_p}{\partial x} + w_p\frac{\partial w_p}{\partial z}\right) = \frac{\partial p}{\partial z} + M_1\delta(1-C)\left(w_f - w_p\right), \tag{22}$$

where $S'$ represents the drag coefficient and $\mu_s$ is used for the empirical representation of liquid's viscosity and is defined as [25]

10.3389/fphy.2023.1111163

$$\left.\begin{aligned} S' &= \frac{9\mu_0}{2a^2}\lambda(C),\\ \lambda(C) &= \frac{4+3\sqrt{8C-3C^2}+3C}{(2-3C)^2},\\ \mu_s &= \frac{\mu_0}{1-\chi C},\\ \chi &= 0.07\exp\left(2.49C+\frac{1107}{T}e^{-1.69C}\right). \end{aligned}\right\} \tag{23}$$

Using Eqs 13 and 14 from Eqs (3) to (12) and imposing the large wavelength assumption along with the minimum Reynold number, the system showing the fluid phase becomes

$$\frac{dp}{dx} = 2\gamma' v_f + (1+\alpha')^{-1}\frac{\partial^2 u_f}{\partial z^2} - M^2(u_f+1) + CM_1(u_p-u_f), \tag{24}$$

$$\frac{\partial^2 v_f}{\partial z^2} = 2\gamma'\left(\frac{\partial u_f}{\partial z}\right)(1+\alpha'), \tag{25}$$

with the non-dimensional boundary conditions being defined as [21]

$$\left.\begin{aligned} \frac{du_f}{dz}(0) = 0, v_f(0) = 0,\\ u_f(h) = -1\\ v_f(h) = 0 \end{aligned}\right\}, \tag{26}$$

where $\gamma = R\Omega a/c$ is the Taylor number, and the particulate phase equation converts to

$$\frac{dp}{dx} = (1-C)M_1(u_f-u_p). \tag{27}$$

The boundary condition physically describes that the axial velocity $u_f$ remains constant at the central line, where $z = 0$ and the flow remains static at the boundary walls due to no slip. On the other hand, the lateral velocity component $v_f$ vanishes at the central axis because of no lateral flow here, and the same is at the walls due to lubricated walls. A compliant wall is described as a wall that has the capacity to contain the liquid and is deformable, stretchy, flexible, and elastic in nature. This wall is flexible and elastic, so when a deforming force is applied to it, it returns to its original shape. A body's ability to self-regulate once external forces that caused deformation, such as those from a sponge, spring, or rubber, are removed is known as elasticity. Contrarily, a material's plasticity refers to its ability to maintain its shape after a deforming force has been withdrawn, as in the case of glass and wood. When applied, a deforming force changes the volume, length, or contour of the wall. The force exerted on the body immediately affects the quantity of change. The word "elastic limit" refers to the maximum amount of force that a wall can withstand before it stops being elastic. If this limit is exceeded, the deformation of the wall will become permanent. All of these elements are monitored in the compliant wall. The compliant wall plays a significant role in fluid movement because it controls the shape of sinusoidal waves during the peristaltic flow. A compliant wall channel's peristaltic non-Newtonian fluid flow was described by [25]

$$2\gamma' v_f + (1+\alpha')^{-1}\frac{\partial^2 u_f}{\partial z^2} + CM_1(u_p-u_f) = E_1\frac{\partial^2\eta}{\partial t^2\partial x} + E_2\frac{\partial^2\eta}{\partial t\partial x} + E_3\frac{\partial^5\eta}{\partial x^5} - E_4\frac{\partial^3\eta}{\partial x^3} + E_5\frac{\partial\eta}{\partial x} + M^2(u_f+1) \tag{28}$$

$$F_1 = \int_0^h \frac{\partial v_f}{\partial z}dz. \tag{29}$$

Eq. (30) suggests that we can choose the remaining two boundary conditions as

$$v(0) = 0, \quad v(h) = F_1. \tag{30}$$

The dimensionless flow rate $F_2$, due to secondary velocity is defined, respectively, as

$$F_2 = \int_0^h v dz. \tag{31}$$

Exact solutions of Eqs (15–19) can be written as

$$u_f = \frac{1}{8\gamma' T_6}\left(\begin{aligned} &-8\gamma' T_6 + 4\gamma'(T_1M^2 - 4T_3\gamma' + T_6T_1)Cosh\left[\frac{T_7 z}{\sqrt{2}\sqrt{1+\alpha'}}\right]\\ &+4\gamma'(-T_1M^2 + 4T_3\gamma' + T_6T_1)Cosh\left[\frac{zT_8}{\sqrt{2}T_5}\right] +\\ &\sqrt{2}\left(\begin{aligned} &(T_4M^2 - 4T_2\gamma' + T_4\gamma')T_5 Sinh\left[\frac{zT_8}{\sqrt{2}T_5}\right] +\\ &(-T_4M^2 + 4T_2\gamma' + T_4\gamma')T_9 Sinh\left[\frac{zT_9}{\sqrt{2}T_5}\right] \end{aligned}\right) \end{aligned}\right), \tag{32}$$

$$u_p = \frac{1}{M_1(1-C)}\left(\begin{aligned} &+4\gamma'^{(-T_1M^2+4T_3\gamma'+T_6T_1)}Cosh\left[\frac{zT_8}{\sqrt{2}T_5}\right]\\ &-8\gamma' T_6 + 4\gamma'(T_1M^2 - 4T_3\gamma' + T_6T_1)Cosh\left[\frac{T_7 z}{\sqrt{2}\sqrt{1+\alpha'}}\right]\\ &+\\ &+\sqrt{2}\left(\begin{aligned} &(T_4M^2 - 4T_2\gamma' + T_4\gamma')T_5 Sinh\left[\frac{zT_8}{\sqrt{2}T_5}\right] +\\ &(-T_4M^2 + 4T_2\gamma' + T_4\gamma')T_9 Sinh\left[\frac{zT_9}{\sqrt{2}T_5}\right] \end{aligned}\right) \end{aligned}\right)\frac{1}{8\gamma' T_6}, \tag{33}$$

$$v_f = \frac{1}{16(-1+C)T^2T_6}\times \left(\begin{aligned} &-8\frac{dp}{dx}\gamma' T_6 + (-1+C)\\ &\left(\begin{aligned} &8T^2(-T_3M^2 + 4T_1\gamma' + T_3T_6)Cos\,h\left[\frac{zT_7}{\sqrt{2}T_5}\right]\\ &\left(\begin{aligned} &\left(\begin{aligned} &T_4M^2 - 2T_2M^2\gamma' - 8T_4T^2 + T_4M^2T_6\\ &-2T_2\gamma'^{T_6} \end{aligned}\right)\\ &T_8\,Sin\,h\left[\frac{zT_8}{\sqrt{2}T_5}\right]\\ &+\left(\begin{aligned} &-T_4M^2 + 2T_2M^2\gamma' + 8T_4T^2 +\\ &T_4M^2T_6 - 2T_2\gamma'^{T_6} \end{aligned}\right)\\ &T_9\,Sin\,h\left[\frac{zT_9}{\sqrt{2}T_5}\right] \end{aligned}\right) \end{aligned}\right) \end{aligned}\right) \tag{34}$$

where constants $T_1 - T_{10}$ are defined as follows

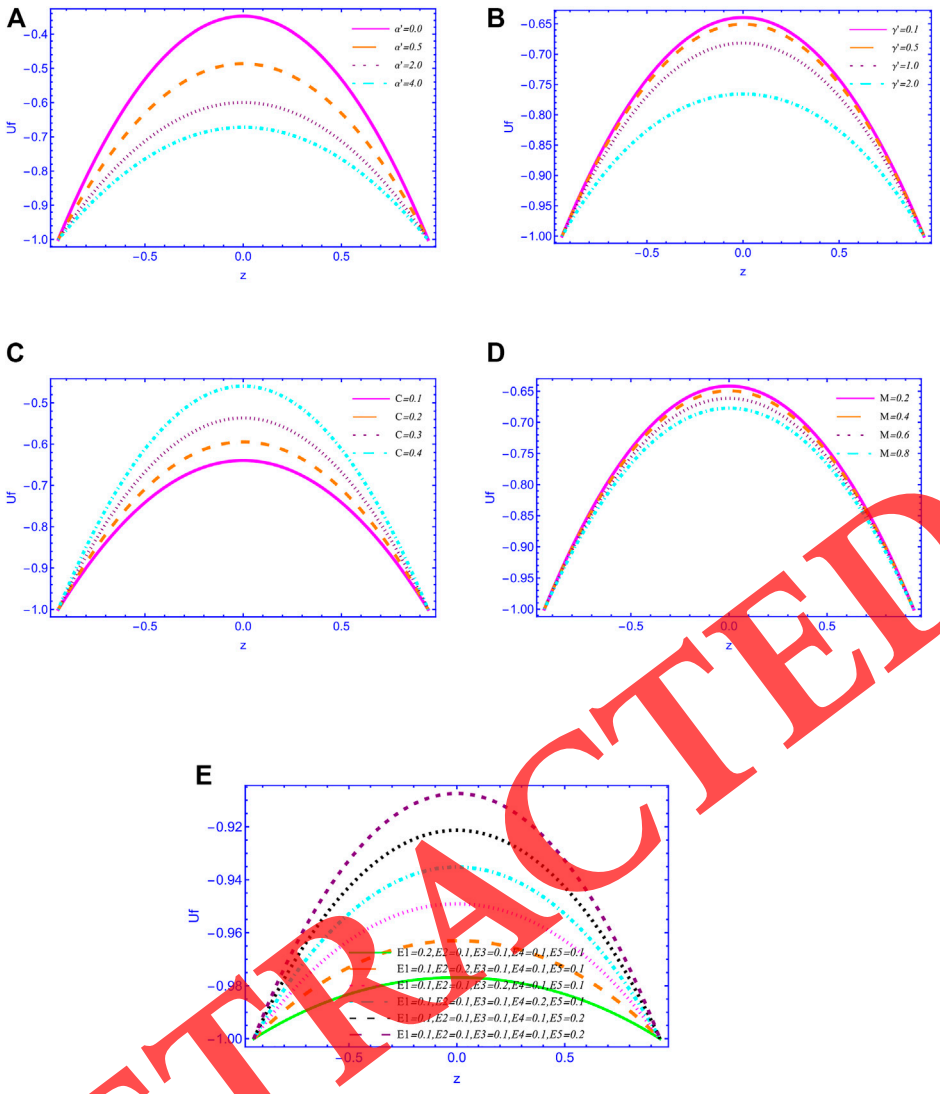


FIGURE 2
**(A)** represents the various values of $\alpha'$ on $u_f$ when $M, C, \gamma' = 0.1$. **(B)** represents the various values of $\gamma'$ on $u_f$ when $M, C, = 0.1, \alpha' = 1.0$. **(C)** represents the various values of C on $u_f$ when $M, \gamma' = 0.1, \alpha' = 1.0$. **(D)** represents the various values of M on $u_f$ when $C, \gamma' = 0.1, \alpha' = 1.0$. **(E)** represents the various values of the compliant wall on $u_f$ when $M, C, \gamma' = 0.1, \alpha' = 1.0$.

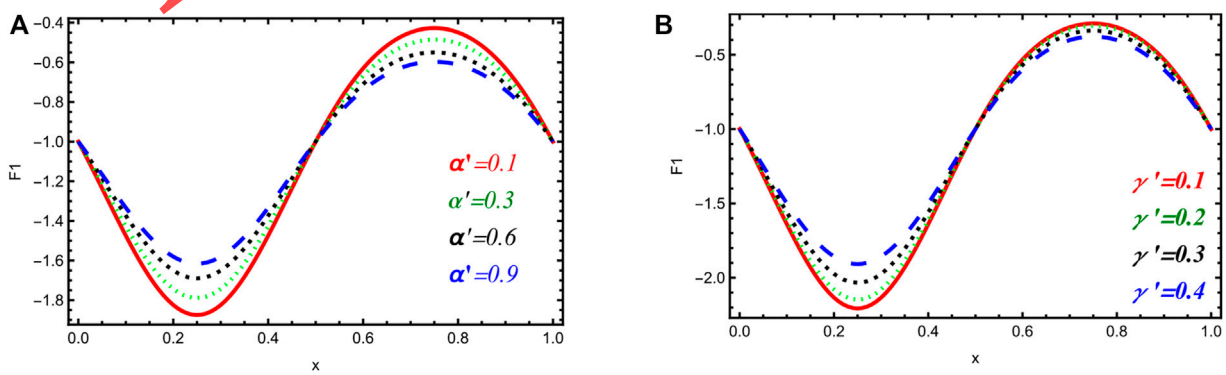


FIGURE 3
**(A)** represents the various values of $\alpha'$ on $F_1$ when $M, C, \gamma' = 0.1$. **(B)** represents the various values of $\gamma'$ on $F_1$ when $M, C, = 0.1, \alpha' = 1.0$.

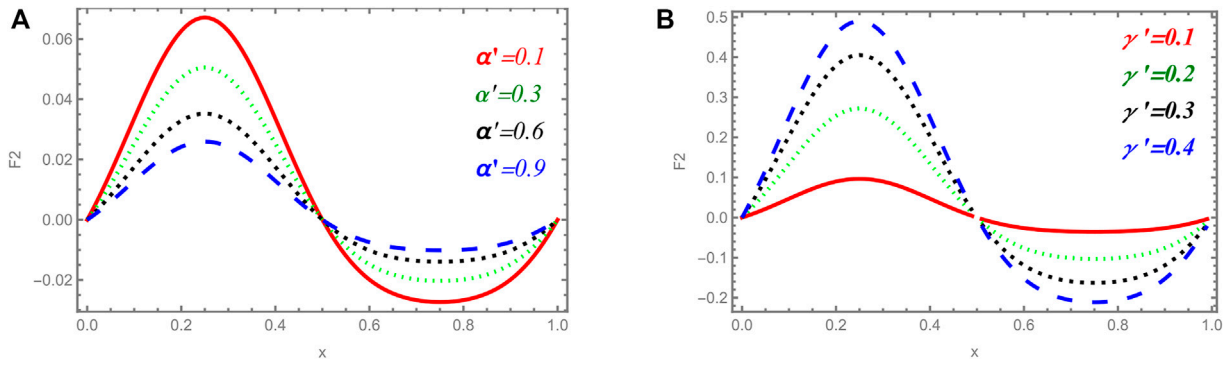


FIGURE 4
**(A)** represents the various values of $\alpha'$ on $F_2$ when $M, C, \gamma' = 0.1$. **(B)** represents the various values of $\gamma'$ on $F_2$ when $M, C, = 0.1, \alpha' = 1.0$.

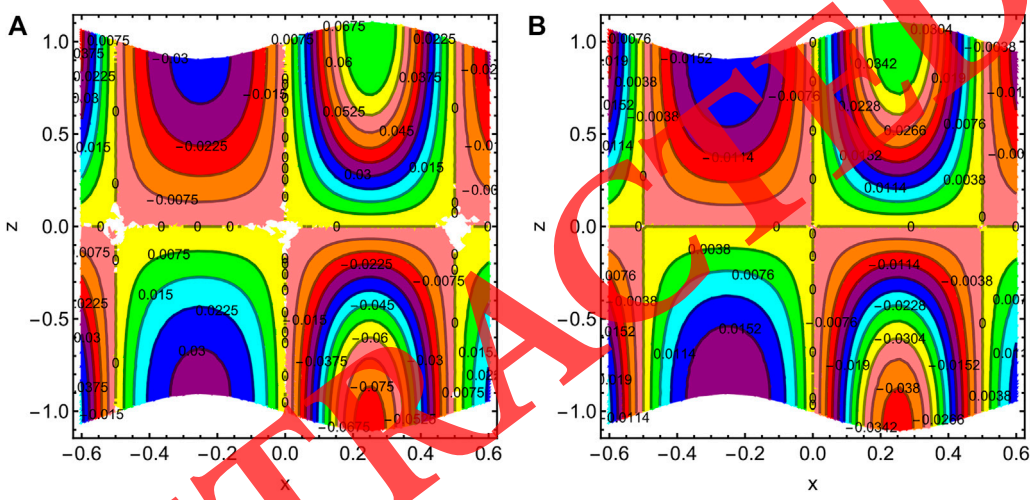


FIGURE 5
**(A, B).** Stream lines of $u_f$ for various values of $M = 1.0$ and $2.0$.

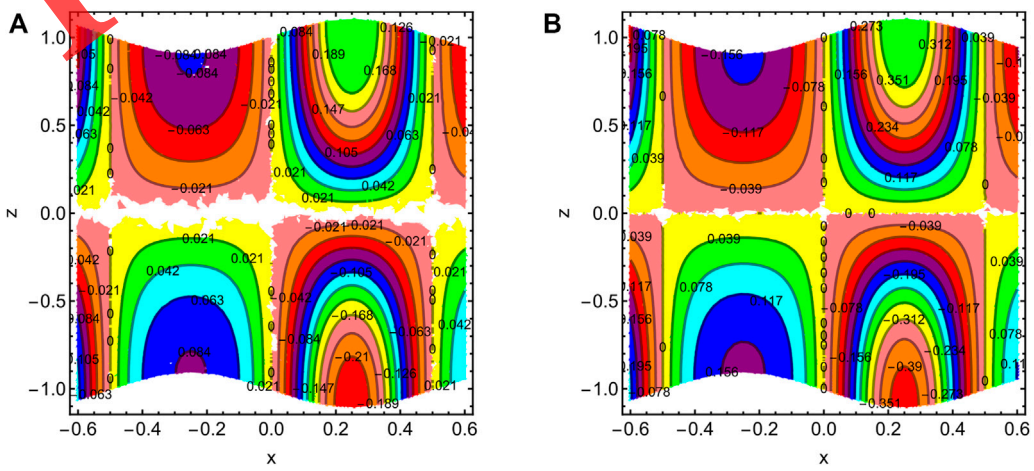


FIGURE 6
**(A, B).** Stream lines of $u_f$ for various values of $\gamma' = .2$ and $.4$.

10.3389/fphy.2023.1111163

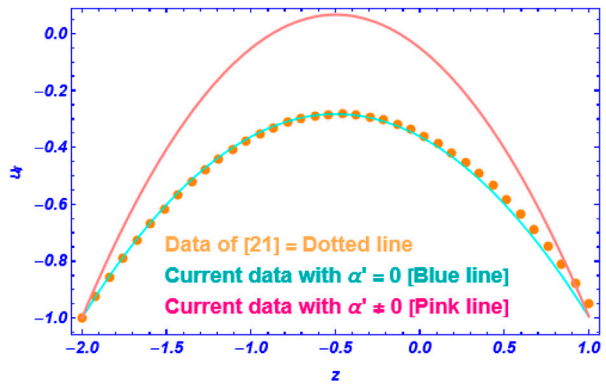


FIGURE 7
Comparison of current results with the existing literature.

$$T_1 = \frac{1}{(-1+C)T_6}\frac{dp}{dx}\left(Cos\,h\left[\frac{hT_7}{\sqrt{2}\sqrt{1+\alpha'}}\right] - Cos\,h\left[\frac{hT_{10}}{\sqrt{2}T_5}\right]\right)Sech\left[\frac{hT_7}{\sqrt{2}\sqrt{1+\alpha'}}\right],$$

$$T_2 = 0,$$

$$T_3 = \frac{1}{4(-1+C)\gamma' T_6}\frac{dp}{dx}\begin{pmatrix} M^2\,Cos\,h\left[\frac{hT_7}{\sqrt{2}\sqrt{1+\alpha'}}\right] + \\ T_6\,Cos\,h\left[\frac{hT_7}{\sqrt{2}\sqrt{1+\alpha'}}\right] \\ -M^2\,Cos\,h\left[\frac{hT_{10}}{\sqrt{2}T_5}\right] \\ +T_6\,Cos\,h\left[\frac{hT_{10}}{\sqrt{2}T_5}\right] \end{pmatrix} Sech\left[\frac{hT_7}{\sqrt{2}\sqrt{1+\alpha'}}\right]Sech\left[\frac{hT_{10}}{\sqrt{2}T_5}\right],$$

$$T_4 = 0, T_5 = \sqrt{1-\alpha'}, T_6 = \sqrt{M^4 - 16\gamma'^2}, T_7 = \sqrt{M^2+T_6}, T_8 = \sqrt{-(-M^2+T_6)T_5},$$

$$T_9 = \sqrt{(M^2+T_6)T_5}, T_{10} = \sqrt{(M^2-T_6)T_5}.$$

## 3 Results

To establish a geometrical discussion on the achieved results from the aforementioned problem, a graphical section is added which provides a variation scenario of various physical quantities against some contributing parameters of the study. The simplified governing equations for the peristaltic movement of the rotating solid particle fluid having compliant walls being tackled in the presence of applied magnetohydrodynamics. The analytical solutions have been attained for both fluid and particulate phase velocity mechanisms. In addition, the expressions for flow rates are measured for both velocity profiles. Figures 2A–E consist of the fluid phase velocity $U_f$ against the Taylor number $\alpha'$, fluid parameter $\gamma'$, solid particle concentration C, Hartman number M, and the compliant walls' parameter. The flow rate $F_1$ can be reported in Figures 3A, B and $F_2$ in Figure 4A, B. Streamlines have been presented through closed contours in Figures 5, 6.

Figure 2A shows that the velocity of the fluid goes on decreasing with large values of the rotational parameter, and the maximum velocity is observed at the center, which suggests physically that the rotational effects will control the flow speed and the fluid molecules collide with each other and also with the channel walls to maintain the flow speed. It is also noticed that the maximum velocity is reported in the case when there is no rotation, i.e., $\alpha' = 0$. The graph of the fluid parameter for the velocity of the fluid phase is shown in Figure 2B, which suggests that velocity is a decreasing function of the fluid parameter $\gamma'$. It is also to be noted here that for the range $0 < \gamma' < 1$, the variation is very minor, but it becomes significant for higher values. The viscosity measures for the non-Newtonian fluid (Ree–Eyring-Powell) are variable and mostly non-linear, as compared to the viscous fluid, which is why the fluid gets thicker with time, and its increasing concentration will create slower flow. It is evident from Figure 2C that velocity flourishes with the increasing impact of solid particle concentration C, and a forward flow can occur by a larger concentration of the particles. It is mostly seen in the physical phenomena of multiphase flows that the presence of solid particles increases the flow intensity by creating extra pressure on the fluid molecules; Figure 2D shows an inverse relationship between velocity and the magnetic field factor $M$ because magnetic field acts as a body force on the fluid's particle to keep the flow relatively slower. It can be seen from Figure 2E that compliant walls are producing fast flow by varying their considerable parameters like $E_1$, $E_2$, $E_3$, $E_4$, and $E_5$. It is found convenient with the physical aspect that elastic properties help in making the flow fast.

The flow rate $F_1$ of the fluid phase against the axial coordinate $x$ has been sketched in Figure 3A for the factor $\alpha'$. It is received from this diagram that in region $R_1$, i.e., $x \in [0, 0.5]$, the flow rate is an increasing function of Taylor's number and in the region $R_2$, i.e., $x \in [0.5, 1]$, the situation is quite the opposite. With the increasing impact of the fluid factor $\gamma$, the flow rate becomes large in region $R_1$ but declines in region $R_2$, as seen in Figure 3B. It is also depicted that the curves are changing their concavity at the point of inflection $x = 0.5$. Figure 4A reveals the flow rate $F_2$ of the particulate phase near the vibrational impact of the Taylor number $\alpha'$. It is concluded from here that the flow rate is varying inversely in region $R_1$, but direct variation is reported in region $R_2$. From Figure 4B, opposite readings are collected for the factor of fluid $\gamma'$. It is summarized that the maximum flow rate is picked at $x = 0.3$, while the minimum is calculated at $x = 0.8$.

Figures 5A, B show streamlines of the fluid phase for various values of the magnetic field $M$. It can be seen that the change of bolus shapes can be found in four quadrants of the plane. If we see in the first quadrant, circulating boluses are expanding in size; in the second quadrant, a rise in the shape is observed and the number of boluses is calculated. In the third quadrant, the size of the bolus decreases, but the number of boluses is increasing, while in the fourth sector, the size and number vary randomly. Figures 6A, B define the streamlines for the fluid parameter $\gamma'$, and it can be noticed that there is no conclusive change in the shape and number of closed contours in the first quadrant, but in the second quadrant, the size of the bolus increases with a larger impact of $\gamma'$. In the third quadrant of the plane, it is computed that the size and number of trapping bolus are reduced accordingly; however, no proper variation is appealing in the fourth portion as well. A comparison of the current study with the previous literature [21] can be found in Figure 7.

## 4 Conclusion

In the current work, we have analyzed the magnetic field effects on the multiphase wavy flow of the Ree–Eyring–Powell fluid in a three-dimensional rotating channel under the constraints of a long wavelength. The flow is assumed to be steady and incompressible. A mechanism of compliant walls is taken into consideration. After using suitable transformations, the governing non-linear equations have been made linear and then solved explicitly by an exact method. Graphical aspect is presented for velocities, flow rates, and trapping

phenomenon. From graphical results and discussion, the summary of the study is described as follows:

- Fluid phase velocity is decreasing the function of rotation, fluid's non-Newtonian property, and the externally applied magnetic field, but a direct relation is reported for the solid particle concentration and compliant wall factors.
- It is declared that the fluid phase flow rate depends inversely on the rotational parameter, the fluid's factor, and the magnetic factor on the left side but increases on the right side.
- It is concluded that solid particles and the fluid phase flow rate are varying directly in the left portion of the axial domain, while the right side reflects the opposite behavior.
- It is availed that the particulate phase flow rate is inversely varying with rotational effects and magnetic effects on the left portion, but the fluid parameter and solid particle concentration are imposing a direct effect on the said profile.
- It is further framed that opposite readings are gathered in the right half of the flow domain.
- It is found that streamline boluses are expanded in the left portion by increasing the magnetic parameter randomly, while the expanded nature remains constant for the fluid parameter.

## Data availability statement

The raw data supporting the conclusion of this article will be made available by the authors, without undue reservation.

## Author contributions

All authors listed have made a substantial, direct, and intellectual contribution to the work and approved it for publication.

## Acknowledgments

The authors would like to thank the Deanship of Scientific Research at Umm Al-Qura University for supporting this work by Grant Code: (22UQU4310392DSR32).

## Conflict of interest

The authors declare that the research was conducted in the absence of any commercial or financial relationships that could be construed as a potential conflict of interest.

## Publisher's note

All claims expressed in this article are solely those of the authors and do not necessarily represent those of their affiliated organizations, or those of the publisher, the editors, and the reviewers. Any product that may be evaluated in this article, or claim that may be made by its manufacturer, is not guaranteed or endorsed by the publisher.



## References

1. Shapiro AH, Jaffrin MY, Weinberg SL. Peristaltic pumping with long wavelengths at low Reynolds number. *J Mech* (1969) 37(4):799–825. doi:10.1017/s0022112069000899

2. Ramachandra Rao A, Mishra M. Nonlinear and curvature effects on peristaltic flow of a viscous fluid in an asymmetric channel. *cta Mechanica* (2004) 168(1):35–59. doi:10.1007/s00707-004-0079-0

3. Munawar S, Saleem N, Aboura K. Second law analysis in the peristaltic flow of variable viscosity fluid. *nt J Exergy* (2016) 20(2):170–85.

4. Pandey SK, Tripathi D. Influence of magnetic field on the peristaltic flow of a viscous fluid through a finite length cylindrical tube. *Appl Bionics Biomech* (2010) 7(3):169–76. doi:10.1080/11762322.2010.490041

5. Sadaf H, Nadeem S. Analysis of combined convective and viscous dissipation effects for peristaltic flow of Rabinowitsch fluid model. *J Eng* (2017) 14(1):182–90. doi:10.1016/s1672-6529(16)60389-x

6. Koriko OK, Adegbie KS, Shah NA, Animasaun IL, Olotu MA. Numerical solutions of the partial differential equations for investigating the significance of partial slip due to lateral velocity and viscous dissipation: The case of blood-gold arreau nanofluid and dusty fluid. *Numerical methods for partial differential equations* (2021). doi:10.1002/num.22754

7. Fetecau C, Ali Shah NA, Vieru D. General solutions for hydromagnetic free convection flow over an infinite plate with Newtonian heating, mass diffusion and chemical reaction. *Commun Theor Phys* (2017) 68(6):768. doi:10.1088/0253-6102/68/6/768

8. Alhazmi SE, Imran A, Awais M, Abbas M, Alhejaili W, Hamam H, et al. Thermal convection in nanofluids for peristaltic flow in a nonuniform channel. *Scientific Rep* (2022) 12(1):12656–19. doi:10.1038/s41598-022-16600-w

9. Adel M, Assiri TA, Khader MM, Osman MS. Numerical simulation by using the spectral collocation optimization method associated with Vieta-Lucas polynomials for a fractional model of non-Newtonian fluid. *Results Phys* (2022) 41:105927. doi:10.1016/j.rinp.2022.105927

10. Rashid M, Ansar K, Nadeem S. Effects of induced magnetic field for peristaltic flow of Williamson fluid in a curved channel. *Physica A: Stat Mech its Appl* (2020) 553:123979. doi:10.1016/j.physa.2019.123979

11. Khan LA, Raza M, Mir NA, Ellahi R. Effects of different shapes of nanoparticles on peristaltic flow of MHD nanofluids filled in an asymmetric channel. *J Therm Anal Calorim* (2020) 140(3):879–90. doi:10.1007/s10973-019-08348-9

12. Sucharitha G, Lakshminarayana P, Sandeep N. Joule heating and wall flexibility effects on the peristaltic flow of magnetohydrodynamic nanofluid. *Int J Mech Sci* (2017) 131:52–62. doi:10.1016/j.ijmecsci.2017.06.043

13. Srinivas S, Kothandapani M. The influence of heat and mass transfer on MHD peristaltic flow through a porous space with compliant walls. *Appl Comput* (2009) 213(1):197–208. doi:10.1016/j.amc.2009.02.054

14. Ashraf MZ, Rehman SU, Farid S, Hussein AK, Ali B, Shah NA, et al. Insight into significance of bioconvection on mhd tangent hyperbolic nanofluid flow of irregular thickness across a slender elastic surface. *Mathematics* (2022) 10(15):2592. doi:10.3390/math10152592

15. Raza M, Ellahi R, Sait SM, Sarafraz MM, Shadloo MS, Waheed I. Enhancement of heat transfer in peristaltic flow in a permeable channel under induced magnetic field using different CNTs. *J Therm Anal Calorim* (2020) 140(3):1277–91. doi:10.1007/s10973-019-09097-5

16. Nazeer M, Irfan M, Hussain F, Siddique I, Khan MI, Guedri K, et al. Analytical study of heat transfer rate of peristaltic flow in asymmetric channel with laser and magnetic effects: Remedy for autoimmune disease. *nt J Mod Phys B* (2022) 37:2350025. doi:10.1142/s021797922350025x

17. Lou Q, Ali B, Rehman SU, Habib D, Abdal S, Shah NA, et al. Micropolar dusty fluid: Coriolis force effects on dynamics of MHD rotating fluid when Lorentz force is significant. *Mathematics* (2022) 10(15):2630. doi:10.3390/math10152630

18. Hasona W, Almalki N, ElShekhipy A, Ibrahim M. Combined effects of thermal radiation and magnetohydrodynamic on peristaltic flow of nanofluids: Applications to radiotherapy and thermotherapy of cancer. *urr Nanoscience* (2020) 16(1):121–34. doi:10.2174/1573413715666190318161351

19. Hayat T, Rafiq M, Ahmad B, Asghar S. Entropy generation analysis for peristaltic flow of nanoparticles in a rotating frame. *nt J Mass Transfer* (2017) 108:1775–86. doi:10.1016/j.ijheatmasstransfer.2017.01.038

20. Hasen SS, Abdulhadi AM. Influence of a rotating frame on the peristaltic flow of a rabinowitsch fluid model in an inclined channel. *J Al-Qadisiyah Comput Sci Math* (2020) 12(1)–21.

21. Haider S, Ijaz N, Zeeshan A, Li YZ. Magneto-hydrodynamics of a solid-liquid two-phase fluid in rotating channel due to peristaltic wavy movement. *nt J Numer Flow* (2019) 30:2501–16. doi:10.1108/hff-02-2019-0131

22. Mabood F, Abbasi A, Farooq W, Hussain Z. Thermophoresis effect on peristaltic flow of viscous nanofluid in rotating frame. *J Therm Anal Calorim* (2021) 143(3):2621–35. doi:10.1007/s10973-020-10348-z

23. Hafeez M, Rehman S, Oreijah M, Guedri K, Bafakeeh OT. A study on dual solutions for water-based hybrid nanofluids flowing through convergent channel with dissipative heat transport. *J Chem Soc* (2022) 99(11):100758. doi:10.1016/j.jics.2022.100758

24. Choudhari R, Baleanu D, Vaidya H, Prasad KV, Khan MI, Bafakeeh OT, et al. Analysis of multiple slip effects on MHD blood peristaltic flow of Phan–Thien–Tanner nanofluid through an asymmetric channel. *Int J Mod Phys B* (2022) 2350102. doi:10.1142/s0217979223501023

25. Alharbi KAM, Ijaz N, Riaz A, Altaf F, Zeeshan A. On multiphase wavy movements of non-Newtonian effery fluid in a rotating channel with MHD and compliant walls: Exact solutions. *waves in random and complex media* (2022) 1–23. doi:10.1080/17455030.2022.2128230

26. Abdelsalam SI, Mekheimer KS. Couple stress fluid flow in a rotating channel with peristalsis. *Hydrodynamics* (2018) 30(2):307–16. doi:10.1007/s42241-018-0037-2

27. Sharma K. FHD flow and heat transfer over a porous rotating disk accounting for Coriolis force along with viscous dissipation and thermal radiation (2022) 51(5):4377–92. doi:10.1002/htj.22504

28. Ishtiaq F, Ellahi R, Bhatti MM, Alamri SZ. Insight in thermally radiative ilia-riven flow of electrically conducting non-Newtonian effrey fluid under the influence of induced magnetic field. *Mathematics* (2022) 10:2007. doi:10.3390/math10122007

29. Suwa K, Saitoh T, Takehara Y, Sano M, Nobuhara M, Saotome M, et al. Characteristics of ntra-left atrial flow dynamics and factors affecting formation of the vortex flow. *Circ J* (2014) 79:144–52. CJ-14. doi:10.1253/circj.cj-14-0562

30. Arvidsson PM, Kovács SJ, Töger J, Borgquist R, Heiberg E, Carlsson M, et al. Vortex ring behavior provides the epigenetic blueprint for the human heart. *Scientific Rep* (2016) 6(1):22021–9. doi:10.1038/srep22021

31. Töger J, Kanski M, Carlsson M, Kovács SJ, Söderlind G, Arheden H, et al. Vortex ring formation in the left ventricle of the heart: Analysis by 4D flow MRI and Lagrangian coherent structures. *Ann Biomed Eng* (2012) 40(12):2652–62. doi:10.1007/s10439-012-0615-3

32. Fyrenius A, Wigström L, Ebbers T, Karlsson M, Engvall J, Bolger AF. Three dimensional flow in the human left atrium. (2001) 86(4):448–55. doi:10.1136/heart.86.4.448

33. Ijaz N, Zeeshan A, Riaz A, Alhodaly MS. Transport of drugs using complex peristaltic waves in a biological system. *waves in random and complex media* (2022) 1–16. doi:10.1080/17455030.2022.2111031

34. Fatima N. *Advances in fluid ynamics. Lecture otes in echanical ngineering*. Singapore: Springer (2021). doi:10.1007/978-981-15-4308-1_6Solution of as ynamic and wave equations with VIM

35. Zeeshan A, Ijaz N, Riaz A, Mann AB, Hobiny A. Flow of nonspherical nanoparticles in electromagnetohydrodynamics of nanofluids through a porous medium between eccentric cylinders. *Porous Media* (2020) 23(12):1201–12. doi:10.1615/jpormedia.2020024813

36. Fatima N, Ijaz N, Riaz A, ElSayed M, Ali SS. Evaluate asymmetric peristaltic pumping rug arrying image in biological system: Measure multiphase flows in biomedical applications. *valuate Asymmetric Peristaltic Pumping Carrying Image Biol Syst Measure Multiphase Flows Biomed Appl Symmetry* (2022) 14(11):2437. doi:10.3390/sym14112437

37. Zeeshan A, Ijaz N, Bhatti MM. Flow analysis of particulate suspension on an asymmetric peristaltic motion in a curved configuration with heat and mass transfer. *ech Industry* (2018) 19(4):401. doi:10.1051/meca/2018022

38. Rashidi MM, Mahariq I, Alhuyi Nazari M, Accouche O, Bhatti MM. Comprehensive review on exergy analysis of shell and tube heat exchangers. *J Therm Anal Calorim* (2022) 147:12301–11. doi:10.1007/s10973-022-11478-2

39. Fatima N. New homotopy perturbation method for solving nonlinear differential equations and Fisher type equation Proceedings of the IEEE international conference on power, control, signals and Instrumentation engineering. Chennai, India, September 2017. p. 1669–73. doi:10.1109/ICPCSI.2017.8391997

40. Ijaz N, Zeeshan A, Bhatti M. Peristaltic propulsion of particulate non-Newtonian Ree-Eyring fluid in a duct through constant magnetic field. *Alex Eng J* (2018) 57:1055–60. doi:10.1016/j.aej.2017.02.009

41. Zeeshan A, Bhatti MM, Ijaz N, Beg OA, Kadir A. Biologically inspired transport of solid spherical nanoparticles in an electrically-conducting viscoelastic fluid with heat transfer. *Therm Sci* (2020) 24(2 Part B):1251–60. doi:10.2298/tsci180706324z

# Nomenclature

## Symbols

$\tilde{U}, \tilde{V}, \tilde{W}$ velocity components
$\tilde{X}, \tilde{Y}, \tilde{Z}$ Cartesian coordinate
$\boldsymbol{C}$ volume fraction
$u_f$ fluid phase velocity
$u_p$ particulate phase velocity
$b$ wave amplitude
$S^{'}$ drag coefficient
$\boldsymbol{c}$ wave velocity
$\boldsymbol{R_e}$ Reynold number
$\bar{B}, \bar{C}$ material constants
$a$ width of the duct
$\boldsymbol{S}$ drag force
$\boldsymbol{B_0}$ magnetic field
$\boldsymbol{P}$ pressure in the fixed frame
$\mathfrak{R}$ stress tensor
$\boldsymbol{M}$ Hartmann number
$\boldsymbol{E_1}$ tension wall
$\boldsymbol{E_2}$ mass wall
$\boldsymbol{E_3}$ damping nature
$\boldsymbol{E_4}$ rigidity
$\boldsymbol{E_5}$ elasticity

## Greek symbols

$\mu_s$ viscosity of the fluid
$\sigma$ electrical conductivity of the fluid
$\lambda$ wavelength
$\alpha$' Ree–Eyring parameter
$\rho$ fluid density
$\gamma'$ rotation parameter

## Subscripts

$\boldsymbol{f}$ fluid phase
$\boldsymbol{p}$ particulate phase